ORIGINAL ARTICLE

Elucidating the Interaction of Squamostatin A and Xylomaticin with Bcl-xl Protein: A Molecular Docking and Dynamics Study in Ovarian Cancer

Wan Noraini Wan Sulaiman, Kaynat Qurban Khimani, Noraziah Nordin

Department of Medical Sciences I, Faculty of Medicine and Health Sciences, Universiti Sains Islam Malaysia, Persiaran Ilmu, 71800, Nilai, Negeri Sembilan.

ABSTRACT

Introduction: The B-cell lymphoma-extra-large (Bcl-xL) protein has emerged as an essential target in cancer therapeutics due to its pivotal role in regulating apoptosis and cell survival. Bcl-xL protein has been found to be overexpressed and associated to ovarian cancer. It has been targeted by various ligands, including both synthetic and natural compounds. **Materials and methods:**Molecular docking was performed by AutoDock Vina software. The MD simulation for the complexes were conducted using the AMBER 2022.1 package. **Results:** Molecular docking analysis revealed that both squamostatin A and xylomaticin possess good binding affinities of –10.9 kcal/mol and 11.6 kcal/mol, respectively. Detailed analysis of the binding modes showed hydrogen bonds and hydrophobic contacts emphasise the stability of the squamostatin A/Bcl-xL and xylomaticin/Bcl-xL complexes. Our findings on molecular dynamics provided both complexes maintained stable over 100 ns within the Bcl-xL protein with RMSD average value of 1.53 ± 0.20 E (squamostatin A) and 1.13 ± 0.12 E (xylomaticin). **Conclusion:** Computational investigation underlines the potential of squamostatin A and xylomaticin as promising candidates for Bcl-xL-targeted therapies. The good and stable binding interaction were observed, incorporated with their structural stability during molecular dynamics simulations, demand further experimental validation to come up with valuable insights for new drug discovery, particularly in cancer therapeutics.
Malaysian Journal of Medicine and Health Sciences (2025) 21(5): 95-105. doi:10.47836/mjmhs.21.5.13

Keywords: Squamostatin A, Xylomaticin, Bcl-xL, Molecular docking, Molecular dynamics

Corresponding Author:
Noraziah Nordin, PhD
Email: noraziahnordin@usim.edu.my.
Tel : +606-7985022

INTRODUCTION

Ovarian cancer remains a significant challenge in oncology, characterized by late-stage diagnosis and high mortality rates. Current treatment strategies, including chemotherapy often face limitations due to the development of drug resistance, heterogeneous tumor biology, and adverse side effects (1). Specifically, the overexpression of B-cell lymphoma-extra-large (Bcl-xL) protein contributes to the survival of cancer cells and drug resistance (2), making them less susceptible to conventional therapies that rely on inducing apoptosis. This condition causes the cancer cells to evade cell death due to the inhibition of the apoptosis process.

The Bcl-xL is the long isoform of BCL-x, a member of the BCL-2 family of proteins. The BCL-2 family are a family of proteins which are known as regulators of cellular apoptosis (3). Bcl-xL protein that lies within the mitochondria is made up of 233 amino acids containing four BH domains, a loop between BH3 and BH4 and a transmembrane region. It plays a role in regulating the apoptosis pathway as an anti-apoptotic protein that acts via different mechanisms including inhibition of Bax (4). Targeting the BCL-2 family, especially its anti-apoptotic proteins have attracted researchers to develop novel anti-tumour drugs that would increase survival and at the same time minimize the side effects compared with conventional therapies (5). Among the other cancer that has been studied with targeting Bcl-xL as the therapy are colorectal cancer (6), urothelial carcinoma (7), and skin cancer (8). This justifies the development of targeting-Bcl-xL therapy as an effective strategy for ovarian cancer treatment. As Bcl-xL protein is highly expressed in cancer cells compared to normal cells, inhibitors of Bcl-xL protein would have triggered apoptosis and led to cell death. In the present study, the Bcl-xL protein's active site or binding site was targeted with acetogenins that can cause the loss of its function.

Acetogenins, the secondary metabolites from

the Annonaceae family, are characterised by a long aliphatic chain with an α, β-unsaturated γ-lactone ring and tetrahydrofuran (THF) rings (9). They are known to be cytotoxic compounds that induce cell apoptosis, and cell cycle arrest, thus could inhibit cancer cell growth (9). Previous studies showed that acetogenin could play a role as a potential inhibitor of Complex I of the respiratory chain in cancer cells which leads to depletion of ATP (10). Two acetogenins, namely squamostatin A and xylomaticin were simulated as potential inhibitors of Bcl-xL protein in the computational study.

Squamostatin A and xylomaticin were found in Annona species and successfully isolated in the 1990s and 2000, respectively (11-12). Squamostatin A is characterised as non-adjacent bis tetrahydrofuran acetogenin (11), while xylomaticin was described as mono-tetrahydrofuran ring type acetogenins (12). Squamostatin A has revealed anti-proliferative activity against nasopharyngeal carcinoma cell lines (both parental and methotrexate resistance cell lines) through several mechanisms which include induced G2/M accumulation, apoptosis, increased cytosolic and mitochondrial calcium (13). The promising findings from previous experimental studies led to this study that could fill a gap in ovarian cancer treatment by offering potential agents from both acetogenins (squamostatin A and xylomaticin) that target Bcl-xL, particularly, to enhance the therapeutic efficacy and reducing the likelihood of resistance. By elucidating the molecular interactions between these compounds and Bcl-xL, could pave the way for the development of more effective ovarian cancer treatment strategies.

MATERIALS AND METHODS

Protein Structural File Preparation

The Bcl-xL protein structure was retrieved from the RCSB Protein Data Bank (PDB ID: 3ZK6, Resolution: 2.48 Â) (14). The water molecules from Bcl-xL were removed using Discovery Studio Visualiser 2020 (15). Homology modelling of the chain A of the Bcl-xL protein was performed using the SWISS-MODEL server to account for the missing residues, an automated protein structure homology-modelling platform available online (16). The Protein Data Bank (PDB) templates that were available for alignment with the Bcl-xL sequence were used to create a three-dimensional structure based on the highest sequence identity and structural similarity. To reduce potential error in structure prediction, the final model was improved and optimized. Using PROCHECK, a thorough stereochemical examination was carried out to further evaluate the quality and correctness of the modelled structure (17). This tool offered a thorough examination of the backbone structure of the protein, including bond lengths and angles. The dihedral angles (phi and psi) of amino acid residues were assessed using the Ramachandran plot, which was produced as a component of the PROCHECK study. Consequently, allowed, generously allowed, and disallowed areas of the residues were identified. Reliability and validity of the projected Bcl-xL structure were confirmed by a high percentage of residues lying within the favoured and permitted regions of the Ramachandran plot, indicating a well-constructed model. This comprehensive evaluation ensures that the homology model is structurally sound and suitable for further studies, such as docking and molecular dynamics simulations.

Ligand Structures Preparation

The selection of these two acetogenins (squamocin A and xylomaticin) were based on previous reported data which found to be better binding affinities as compared to ABT-737 as the control Bcl-xl inhibitor (18). The structures of squamostatin A (CID: 44591858) and xylomaticin (CID: 10077684) were retrieved from the PubChem and SpectraBase databases, respectively. Using BIOVIA Discovery Studio 2020, the ligands were initially created in three-dimensional structures. Polar hydrogen was added the added, and the non-polar hydrogen atoms from both ACGs were eliminated. Prior to docking work, the ligands were minimised using AutoDock tools version 4.2.6 (19) and the files were finally kept in PDBQT format. All SMILES codes that were obtained were used to screen the drug-likeness and drug bioactive potential of these metabolites.

Validation of Docking and Determination of Active Site

The native ligand, compound 2, obtained from crystal structure of BCL-XL protein was separated and prepared by adding Gasteiger charges and hydrogen atoms. Meanwhile, the modelled protein structure was prepared using AutoDock Tools (ADT) version 1.5.6, which included addition of polar hydrogen atoms and Kollman charges. The co-bound ligand was superimposed to obtain the active site grid box 46Ч54Ч46 and 0.375 E. Autogrid4 and autodock4 programs utilized to perform redocking of the cognate ligand using the validation method of pose selection whereby docking programs are used to re-dock into the target's active site a compound with a known conformation and orientation. The root-mean-square deviation (RMSD) value of <2 E implies that the docking procedure was valid (20). The grid size and coordinates fixed was very similar to the ones reported by Lessene et al. (2013).

Bioactive Compound Screening for Anticancer Activity

The SMILES codes were submitted to the Way2Drug PASS Online website (http://www.way2drug.com/PASSOnline) for screening bioactivity (21). Anticancer activity including, antineoplastic, antioxidant, apoptosis agonist, Caspase 3 stimulant and antimetastatic were predicted. The resulting data were then tabulated and processed as bar graphs for comparison. These data were used for comparison with ligand-protein affinity results. Assuming that a compound is less likely to show activity in an experiment if its activity likelihood potential (Pa) score is less than 0.5; it is likely to show activity in an

experiment if its Pa score is between 0.5 and 0.7; and it is very expected to show activity in an experiment if its Pa score is greater than 0.7 (21).

Molecular Docking for Squamostatin A and Xylomaticin

The molecular docking of squamostatin A and xylomaticin was performed into the active site of Bcl-xL protein via AutoDock Vina version 1.2.0 software. The partial charges for both ligand and protein were assigned based on Gasteiger-Marsili's calculation and Kollmann's charges. It was then followed by the addition of polar hydrogens to the protein and the merging of non-polar hydrogens in the ligands. The docking was set up by positioning the grid box in the targeted pocket via the autogrid4 program. The best conformations were selected and generated using the Lamarckian genetic algorithm (LGA) and the inter-molecular interaction patterns were visualised and analysed from the selected poses (22).

ADME-TOX Profiling of the Bioactive Compounds

Pharmacokinetic properties are essential in drug development as they determine the drug's behavior in the body, influencing its efficacy and safety. These properties encompass absorption, distribution, metabolism, and excretion (ADME), which collectively dictate the drug's bioavailability and therapeutic potential. The SMILES codes of the 2 metabolites were submitted for input in an online drug-likeness test by the Swiss Institute of Bioinformatics: absorption, distribution, metabolism, and excretion test or SwissADME. This test was carried out to observe initial data, which consisted of molecular weight, chemical pharmacokinetic properties, and drug- likeness properties based on Lipinski et al. (1997) and the "rule of five" (LRO5) – including molecular weight ≤ 500 g/mol, octanol-water partition coefficient MLogP ≤ 4.5, hydrogen bond acceptor (N or O) ≤ 10, and hydrogen bond donor (NH or OH) ≤ 5) (23). Bioavailability, in conjunction with the ADME LRO5, describes how a molecule might enter the systemic blood circulation and, consequently, become accessible at the site of action (24), and synthetic accessibility describes the difficulty of the compound to be synthetically manufactured based on its structural complexity (25). The toxicological profiles of two substances, xylomaticin and squamostatin A, were predicted using Toxtree software (26). The Cramer decision tree, which divides substances into three toxicity classifications according to molecular structure, was used to assess both substances. To evaluate any carcinogenic or mutagenic qualities, genotoxicity and nongenotoxicity alarms were also investigated. By entering each compound's structure in SMILES format, Toxtree was able to compare possible toxicity risks consistently.

Molecular Dynamic (MD) Analysis for Squamostatin A and Xylomaticin

The best conformation of ligand and protein from the docking study was further validated by molecular dynamics. The MD simulation for the complexes was conducted using the AMBER 2022.1 package (27). Prior to MD simulation, both ligands (squamostatin A and xylomaticin) were minimised, and partial charges were determined using FLARE V6.1. The parameters of Bcl-xL protein were set by ff19SB (28), while the general Amber force field (GAFF) force field for the ligands (29).

Both complexes were submerged in OPC (Optimized Potential for Liquid Simulations) water molecules in an octahedral box as part of the explicit solvent model. This method allows for the protonation states of ionizable groups to fluctuate, emphasizing the importance of the solvent's role in the simulations. Energy minimisation was performed in squamostatin A/Bcl-xL and xylomaticin/ Bcl-xL using the steepest descent and conjugate gradient minimization (2). The minimisation process was repeated several times to achieve the minimised state and kept unrestrained at the final step of minimisation. It was further continued by a two-step equilibration process in which the equilibrations constant pressure and temperature ensemble (NPT) second step was used in the second step. This process was carried out in applied restrain for ~10 ns with a gradual decrease until no restraint was observed. A production run of 100 ns without any retraining force was conducted in the targeted system once the equilibration was obtained. The Langevin dynamics was used to control temperature, while isotropic position scaling for the pressure. The Particle Mesh Ewald (PME) method was used to compute long-range electrostatic interactions (30), while the SHAKE algorithm was used to constrain the interactions involving H-atom (31).

The visual analysis of simulated trajectories was performed using VMD (32). The binding properties of the ligands were evaluated for a 100 ns production trajectory. The stability metrics including root mean square deviation (RMSD), root mean square fluctuation (RMSF), and analysis of radius of gyration (RoG) and H-bond were accomplished via the CPPTRAJ program (33). The Xmgrace was used to plot the graphs.

RESULTS

Validation of Docking

Docking protocol validation was an essential first step in determining whether the docking procedure was valid and reliable. The RMSD value for native ligand in Bcl-xL was 0.852 Å. Figure 1A shows the results of

superimposing the re-docking ligand (green color) on the native ligand (blue color) and the interaction profile for the co-crystallized ligand.

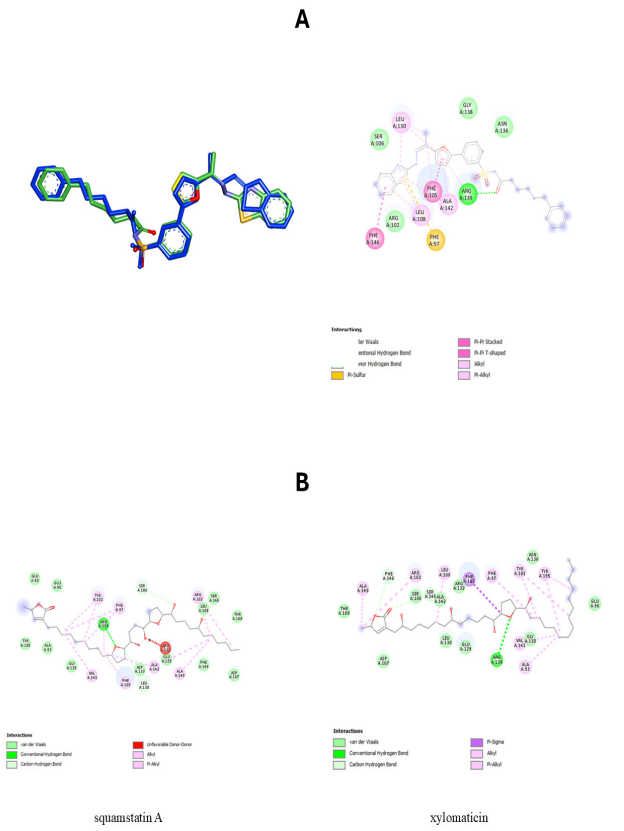

Figure 1: Docked Bcl-xL protein with ligands. (A) compound 2 co-crystallized ligand (Green) superimposed over native ligand (blue) and two-dimensional interaction profile of binding interaction of redocked ligand with Bcl-xL protein. (B) Two-dimensional illustration of binding interaction of the squamstatin A and xylomaticin into Bcl-xL. Different interactions are depicted in dashed lines between ligands and protein residues.

QSAR Assessment for Anticancer Activities

We have also predicted the anticancer spectrum applying web server PASS of the compounds (34). The PASS results are intercepted as Pa and Pi, which are displayed in Table I. As can be seen in Figure 2, xylomaticin and squamostatin A reveals promising anticancer activities with varying probabilities of activity (Pa) and inactivity (Pi) for key cancer-related mechanisms. Both compounds exhibit a high likelihood of functioning as electron transport complex I inhibitors (Pa = 0.721 for xylomaticin and Pa = 0.709 for squamostatin A), indicating potential in disrupting mitochondrial respiration in cancer cells. The antineoplastic activity of both compounds is also notable, with xylomaticin showing Pa = 0.607 and squamostatin A displaying Pa = 0.605, suggesting general anticancer potential. As apoptosis agonists, squamostatin A has a slightly higher Pa (0.493) compared to xylomaticin (0.468), indicating a strong potential to promote programmed cell death in cancer cells. Both compounds also display antimetastatic activity, with similar probabilities (Pa = 0.453 for xylomaticin and Pa = 0.442 for squamostatin A), which could help inhibit cancer cell spread. Interestingly, xylomaticin has a notable probability of activity as a caspase-3 stimulant (Pa = 0.305), a role not predicted for squamostatin A, suggesting an additional apoptotic pathway activation for xylomaticin.

Table I: Prediction of anticancer activity using PASS

Predicted Anticancer Activity	Xylomaticin		Squamostatin A	
	Pa	Pi	Pa	Pi
Electron transport complex I inhibitor	0.721	0	0.709	0
Antineoplastic	0.607	0.043	0.605	0.044
Apoptosis agonist	0.468	0.047	0.493	0.042
Antimetastatic	0.453	0.031	0.442	0.034
Caspase 3 stimulant	0.305	0.123	0	0

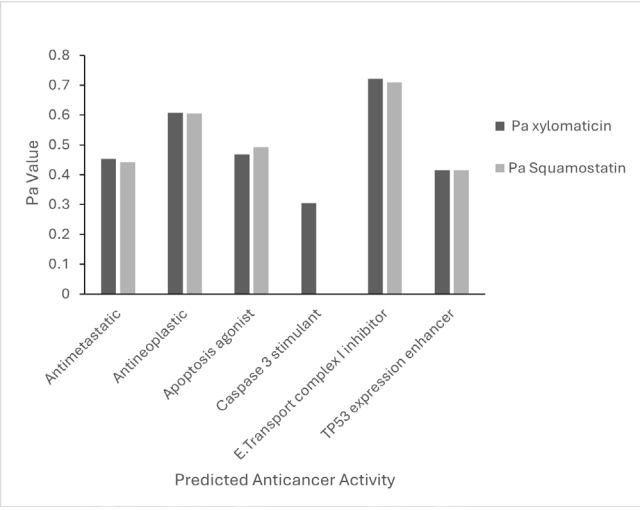

Figure 2: Anticancer activity Prediction graph for Compounds

Docking Squamostatin A and Xylomaticin into Bcl-xL

The docking for squamostatin A and xylomaticin into the Bcl-xL active site was conducted using AutoDock vina. The docking results are presented in Table II and Figure 1B. In the present study, squamostatin A and xylomaticin showed strong binding energies with low binding affinities of –10.9 kcalmol^{-1} and –11.6 kcalmol-$^{-1}$, respectively (Table II). The squamostatin A/Bcl-xL and xylomaticin/Bcl-xL have three H-bonds, one of which is connected to one of the critical residues of Arg139. The Arg139 residue is connected to the gamma lactone of the squamostatin A and xylomaticin with bond lengths of 2.58 Å and 2.84 Å, respectively. The formation of H-bond of squamocin A with Bcl-xL residues was also observed in Ser106 and Leu130 with distances of 3.21 and 3.24 Å, respectively. On the other hand, Ser145 and Phe146 formed the H-bond contact with xylomaticin at 3.47 and 3.53 Å. The formation of the H-bond between squamostatin A with Bcl-xL has the closest distance as compared with xylomaticin for all H-bond formations. Additionally, the xylomaticin/Bcl-xL complex showed more hydrophobic contacts than squamostatin A/Bcl-xl with six similar residues in both complexes, namely

Phe97, Tyr101, Arg102, Phe105, Val141 and Ala149.

Table II: Docking results illustrate the binding affinities and interaction profile of squamostatin A and xylomaticin with Bcl-xL.

Ligand	Binding Affinities (kcalmol^{-1})	Hydrogen Bonding	Hydrophobic Interaction	Electrostatic Interaction
Co-crystallized ligand (HE I1198)	-10.72	Arg139	Leu130,Phe105. Ala102, Leu108,Phe146	Phe197
Squamostatin A	-10.9	Arg139, Ser106, Leu130	Arg102, Arg139, Val141, Ala142, Ala149, Phe97, Tyr101, Phe105	-
xylomaticin	-11.6	Arg139, Ser145, Phe146	Phe105, Ala93, Val141, Ala149, Leu108, Arg102, Phe97, Tyr101, Tyr195	-

*Arg: Arginine, Val: Valine, Ala: Alanine, Phe: Phenylalanine, Tyr: Tyrosine, Leu: Leucine, Ser: Serine

Drug Likeness and Toxicological Profile of the Compounds

The SwissADME analysis of the two compounds, likely representing xylomaticin and squamostatin A, reveals comparable characteristics in their structural complexity and pharmacokinetics. Table III depicts and compares the suitability of both compounds as potential drugs. The high Csp proportion of 0.92 for both compounds suggest a robust three-dimensional structure and enhances target selectivity. However, the low gastrointestinal (GI) absorption and poor water solubility of these compounds may restrict their oral bioavailability. Their inability to function as P-gp substrates suggests a decreased likelihood of efflux-related resistance, which is advantageous for intracellular retention, especially in cancer treatment. Furthermore, these compounds show lower probability of drug-drug interactions by inhibiting the major CYP450 enzymes, except for CYP3A4. Both compounds pass the Brenk and PAINS filters, indicating that there aren't many toxicity issues. Their synthetic accessibility scores (7.62 and 8.0) confirm the feasibility of synthesis using available methods. Furthermore, Toxtree predicted the toxicity profile of the potential leads. Based on their molecular structures, xylomaticin and squamostatin A were both categorized as Cramer Class III (significant), suggesting a significant potential for toxicity. The lack of structural alarms for genotoxic or nongenotoxic carcinogenicity in xylomaticin suggested a decreased risk of direct DNA damage. Nevertheless, Michael Acceptor and SN2 alerts were found, which would indicate cytotoxic tendencies. Similarly, no genotoxic or nongenotoxic alerts were detected for squamostatin A, but no specific alerts like SN2 or Michael Acceptors were identified, suggesting fewer structural concerns for cellular reactivity than xylomaticin.

Table III: Swiss ADME comparison for squamostatin A and xylomaticin candidates

Category	Squamostatin	Xylomaticin	Comparison
Formula	$C_{37}H_{66}O_8$	$C_{37}H_{68}O_7$	Same core size, but squamostatin A has more oxygen (O).
Molecular Weight	638.92 g/mol	624.93 g/mol	Both are heavy molecules (>500 g/mol), leading to Lipinski violations.
TPSA (Polar Surface Area)	125.68 E	116.45 E	Squamostatin A is slightly more polar, impacting solubility and absorption.
Fraction Csp	0.92	0.92	Identical; both have favorable 3D structures, aiding binding affinity.
H-bond Donors / Acceptors	8-Apr	7-Apr	Similar hydrogen bonding potential.
Rotatable Bonds	25	28	Xylomaticin is slightly more flexible, which may affect binding or solubility.
Solubility (Log S ESOL)	-7.18 (Poorly soluble)	-7.85 (Poorly soluble)	Both are poorly soluble, but squamostatin A has slightly better solubility.
GI Absorption	Low	Low	Both have limited gastrointestinal absorption.
BBB Permeant	No	No	Neither compound crosses the blood-brain barrier.
CYP3A4 Inhibition	Yes	Yes	Both inhibit CYP3A4, potentially affecting drug metabolism.
Other CYP Inhibition	None	None	Both avoid inhibition of other CYP enzymes, reducing drug interaction risks.
P-gp Substrate	No	No	Neither is a P-gp substrate, suggesting low efflux risk.
Log P (Consensus)	6.72	7.66	Xylomaticin is more lipophilic, which may enhance permeability but reduce solubility.
Lipinski Violations	1 (MW > 500)	1 (MW > 500)	Both violate Lipinski's rule due to high molecular weight.
Bioavailability Score	0.55	0.55	Both have moderate bioavailability potential.
PAINS / Brenk Alerts	0 / 0	0 / 0	No structural alerts for toxicity or assay interference for either.
Synthetic Accessibility	7.62	7.62	Both are equally complex but synthetically feasible.

BB: Blood Brain Barrier, GI; Gastrointestinal

Molecular Dynamics (MD) of Squamostatin A/Bcl-xL and Xylomaticin/Bcl-xL Complexes

Squamostatin A/Bcl-xL and xylomaticin/Bcl-xL complexes were simulated for molecular dynamics to examine the consistency and validate the docking interaction of both complexes. The stability and possible deviation were analysed through the Root-Mean-Square Deviation (RMSD) calculation of all the C atoms (Figure 3A). Both complex systems have attained stability within 100 ns of MD simulation. The average RMSD obtained for squamostatin A was 1.53 ± 0.20, while xylomaticin was 1.13 ± 0.12 Å. Both tested ligands exhibited good stability with no significant difference between both complexes.

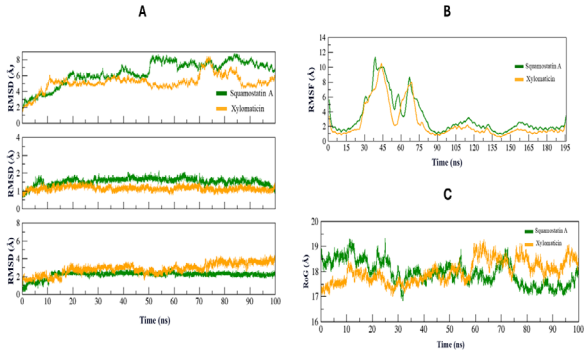

Figure 3: Bcl-xL docked with squamostatin A and xylomaticin in 100 ns simulation. (A) RMSD for whole protein (upper), without loops (middle) and ligands (bottom). (B) RMSF values over MD simulation of squamostatin A and xylomaticin into Bcl-xL protein. (C) Radius of Gyration (RoG) in MD simulation trajectory.

Both complexes revealed that the ligands underwent fluctuations in their orientations within the binding pocket over the MD simulation in the Root-Mean-Square-Fluctuations (RMSF) (Figure 3B). Some residues, such as Gly39 and Tyr40 interact with squamostatin A with a great fluctuation with values of 10.61 and 11.39 Å, respectively. Similarly, xylomaticin/Bcl-xL complex displayed dynamic interactions between the ligand and the protein with some bigger fluctuations within the binding pocket at residues Met45 and Glu46 with values of 10.49 and 9.59 Å, respectively. The average RMSF recorded for squamostatin A/Bcl-xL and xylomaticin/Bcl-xL complexes were 3.15 ± 2.39 and 2.44 ± 2.24 Å, respectively. The prediction of the Radius of Gyration (RoG) as shown in Figure 3C exhibited that squamostatin A/Bcl-xL and xylomaticin/Bcl-xL complexes display similar average RoG values with 17.95 ± 0.47 E and 18.0 ± 0.44 Å, respectively.

Inter-Molecular Interaction Pattern

The analysis of inter-molecular interaction was done following the completion of simulation run. In the case of squamostatin A, our findings reveal that crucial residue, such as Ser106, Leu130 and Arg139 are involved in forming hydrogen bonds, whilst other residues formed hydrophobic interactions with the Bcl-xL protein (Figure 4). Similarly, hydrogen bond profile for xylomaticin highlighted the importance of specific amino acid residues, namely Arg139 which contributes in the formation of stable hydrogen bonds with Bcl-xL.

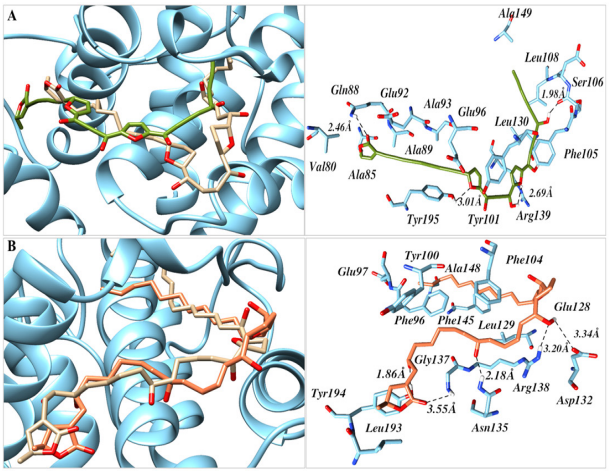

Figure 4: Intermolecular interaction diagram of the ligands in complex with Bcl-xL. [A] Squamostatin A. [B] Xylomaticin. The left side section represents the superimposition of the starting structures (Stick model) and the binding poses during the terminal stages of MD simulation. The detailed pattern is depicted in the right-side panel.

DISCUSSION

The study of molecular interactions between small molecules and proteins is a fundamental aspect of drug discovery and structural biology. In this study, we conduct the simulation of molecular docking and molecular dynamics of two natural acetogenins, squamostatin A and xylomaticin, within the binding site of the Bcl-xL protein. These investigations have provided important insights into the potential of these compounds as inhibitors of Bcl-xL and their structural stability within the protein's binding pocket. The Quantitative structure activity relationship QSAR of the lead compounds revealed the biochemical indicators of anticancer activity as presented in Table II.

In accordance with studies involving similar compounds, both compounds have a high possibility of functioning as electron transport complex I inhibitors, a mechanism associated with the selective toxicity of cancer cells due to mitochondrial malfunction (35).Theprojected antineoplastic action for both supports their broad anticancer potential as they are consistent with previous studies on their cytotoxic effects against particular cancer cell lines (36). Interestingly, xylomaticin shows caspase-3 stimulation activity, which indicates a potential for promoting apoptosis via the caspase pathway. According to studies done by Srivastava & Saxena (2023), substances that activate caspase-3 tend to tend to induce stronger apoptosis in cancer cells, indicating xylomaticin's efficacy in malignancies that depend on this pathway (37). Despite not being predicted to be a caspase stimulant, squamostatin A exhibits somewhat better efficiency as an apoptosis agonist., indicating a more generalized apoptotic effect,

as observed in earlier studies (38).

Both compounds possess antimetastatic properties, which are beneficial in halting the spread of cancer. This possibility is consistent with prior research establishing that natural compounds with complex structures can inhibit metastatic processes (39). These combined results highlight xylomaticin and squamostatin A's potential as versatile anticancer agents, though further experimental validation is necessary to confirm these mechanisms and refine their pharmacokinetics. Preceding the prediction of sufficient anticancer activity of the compounds with Pa > 0.3, The initial simulation was performed through molecular docking which serves as a valuable step in understanding the binding affinity and modes of interaction between ligands and their protein targets (40).

As shown in Table I, both squamostatin A and xylomaticin exhibited strong binding affinities for the Bcl-xL protein. Their binding affinities are comparable and even stronger than ABT-737 (- 9.2 kcalmol-1), as a standard ligand of Bcl-xL (28). A study conducted by Ghani et al (2020) on flavonoids against Bcl-xL showed that the highest binding affinity recorded was fisetin/Bcl-xl protein complex (−8.8 kcalmol-1) (41). This finding showed that squamocin and xylomaticin from acetogenin group in the current study has better interaction as compared to flavonoids. Among the residues that both ligands shared similarity is Arg139. The critical function of the Arg139 residue positioned within the hydrophobic groove pockets at P2 and P4 of the Bcl-xL protein is crucial in the high-affinity binding with proapoptotic and BH3-only proteins (13, 30). Within these P2 and P4 pockets, there are various amino acids, including Glu96, Tyr101, Ser106, Asp107, Leu108, Arg139, and Tyr195 that play key roles (30). Notably, the P2 hydrophobic pocket, characterized by its deep and adaptable structure, demonstrates a more robust affinity for ligand molecules when compared to the P4 pocket (31).

A notable aspect of the molecular docking results was the identification of key binding interactions. Both squamostatin A and xylomaticin displayed hydrogen bonds and hydrophobic contacts with residues within the Bcl-xL binding pocket (Figure 1B). As the H-bond plays an important role in the formation of complexes between macromolecules and small molecules, it occurs when there is interaction with a highly electronegative atom like oxygen, nitrogen, or fluorine within the protein (13). Another interaction found in both complexes is hydrophobic contact. The residues of Bcl-xL that interacted with squamostatin A and xylomaticin also interacted hydrophobically with ABT-737, namely Tyr101 and Phe105 (18). The same residues were reported in various inhibitors from previous studies within the hydrophobic groove of chain A within the crystalised Bcl-xL template (42).

Understanding pharmacokinetics is essential for predicting drug behaviour and ensuring successful therapeutic outcomes. Xylomaticin and squamostatin A exhibit promising features as potential anticancer drug candidates, supported by their favorable structural and pharmacokinetic profiles. The three- dimensional structural complexity of xylomaticin is enhanced by its high Csp percentage (0.92), which improves target specificity and reduces off target effects.

Due to the absence of PAINS and Brenk alerts, SwissADME results indicate a low probability of adverse interactions, indicating a low toxicity risk and a lower possibility of false positives in biological screening (43). The molecules also demonstrate a bioavailability score of 0.55, pointing to a reasonable potential for oral administration that can be optimized further for enhanced absorption. Efflux related resistance, a prevalent issue in cancer treatment that compromises intracellular drug retention, is decreased by xylomaticin's non-substrate status as a P-gp (44). Similarly, Squamostatin A has gained attention as a prospective anticancer agent, with SwissADME data reflecting its moderate oral bioactivity and potential for optimization.

With a synthetic accessibility score of 7.62, squamostatin A is a viable candidate for additional preclinical research since it may be produced using readily available chemical technique (45). Additionally, Squamostatin A does not act as a P-gp substrate, which could help circumvent drug resistance by enhancing intracellular accumulation in cancer cells (46). While squamostatin A's high molecular weight and solubility present challenges, its selective inhibition of CYP3A4 without significant impact on other CYP enzymes helps minimize drug-drug interactions, allowing for a stable metabolic profile comparable with xylomaticin (44). Together, xylomaticin and squamostatin exhibit considerable amounts of potential as anticancer drugs, and important SwissADME indicators suggest that they may be effectively optimized to overcome existing obstacles in cancer therapy. Although the toxicological profile for the compounds seems unfavorable in the analysis, this category aligns with findings for similar natural products known for complex bioactivity and cytotoxicity potential (46).

However, there are subtle variations in their toxicological profiles regarding specific alarms. Neither compound exhibited genotoxic nongenotoxic alerts, which implies a reduced likelihood of directly inducing DNA mutations or cancerous changes. This is consistent with research on structurally comparable bioactive chemicals and implies that neither substance has rapid genotoxic hazards (47). The presence of SN2 and Michael Acceptor alerts in xylomaticin suggests a higher risk for cellular reactivity compared to squamostatin A. Because of their tendency to interact with nucleophiles

in biological systems, these functionalities are frequently linked to increased cytotoxicity, which may result in oxidative stress or interfere with cellular processes (48). These results indicate that while the compounds show promise in terms of safety and target specificity, further optimization is required to enhance their bioavailability and solubility for effective therapeutic applications.

Conversely, molecular dynamics simulations provided valuable insights into the dynamic behaviour and stability of squamostatin A and xylomaticin within the Bcl-xL protein over time. The stability of these complexes during the simulation period is important when considering their potential as therapeutic agents. Initially, the RMSD for both complexes gradually increased until 10 ns and remained constant after 20 ns for xylomaticin/Bcl-xL, while squamostatin A showed an increasing pattern towards 100 ns (Figure 3A). The conformational changes and flexibility exhibited by the squamostatin A and xylomaticin ligands suggest that the ligands binding induces local structural rearrangements, which could have functional implications for the inhibition of Bcl-xL activity (49).

Significant fluctuation was shown by the complex of squamostatin A/Bcl-xL and xylomaticin/Bcl-xL in some residues (Figure 3B), exhibiting dynamic side-chain motions with the ligand. Meanwhile, the prediction of RoG of both complexes is a crucial step in comprehending their structural characteristics and functional implications. By computing the RoG (Figure 3C), the overall compactness and flexibility of the complex can be assessed (49), which shows the significant potential for squamostatin A and xylomaticin in drug design to interact with Bcl-xL. The analysis of inter-molecular interaction in Figure 4 plays a vital role in stabilising the squamostatin A/Bcl-xL and xylomaticin/ Bcl-xL complexes. The unique chemical structures of squamostatin A and xylomaticin dictate their specific binding preferences within the Bcl-xL binding pocket. Our investigation into the inter-molecular interaction patterns of squamostatin A and xylomaticin binding into Bcl-xL revealed that their structure plays a role in protein selectivity (50). These findings suggest plausible avenues for the design of novel small molecules with potent biological activities targeting Bcl- xL which has contributed significantly to the field of protein-ligand interactions (50).

Overall, molecular dynamics simulations of squamostatin A/Bcl-xL and xylomaticin/ Bcl-xL complexes have shown the dynamic nature of the interactions between these acetogenins and the Bcl-xL protein. These insights increase our understanding of the structural activity relationship and pharmacological profile of the selected acetogenin compounds and reveal the binding mechanisms and conformational changes that led to the stability and specificity of these protein-ligand interactions. Importantly, these findings suggest in-silico prediction of novel therapeutic strategies targeting Bcl-xL as its inhibitors with improved binding kinetics and potency as antineoplastic agents.

CONCLUSION

The *in silico* drug activity profile together with interactions and stability of squamostatin A and xylomaticin within the Bcl-xL protein's binding pocket have been illustrated by the current study. Both squamostatin A and xylomaticin had high binding affinities of - 10.9 and -11.6 kcalmol-1, respectively, to the Bcl-xl protein, which suggests that they could be effective ligands for modifying Bcl-xL activity. The binding modes exhibited by these acetogenins showed strong binding interactions by three hydrogen bonds in which one of the interactions are with Arg139 as a critical residue for the inhibition process of Bcl-xL. Squamostatin A and xylomaticin observed stable binding without dissociation within the Bcl-xL protein during the simulation period of 100 ns, according to the trajectories from molecular dynamics simulations, with few changes in their RMSD. This suggests the robustness of these interactions and their potential to be developed as a new Bcl-xL-targeted therapeutic with slight modifications to mitigate the toxicity and increase their bioavailability. Our computational analysis of squamostatin A and xylomaticin has provided some insights into the antineoplastic profiles of these compounds and it is suggested that additional experimental validation, including *in vitro* and *in vivo* studies to confirm the biological activity and therapeutic potential in the future drug development process.

ACKNOWLEDGEMENT

We wish to acknowledge Universiti Sains Islam Malaysia for the financial support granted under the PPP grant (PPPI/FPSK/0121/USIM/16421) to conduct this research. We would like to express our gratitude to Michele Cosi from University of Arizona for his guidance and technical support of the simulation software.

REFERENCES

1. Havasi A, Cainap SS, Havasi AT, Cainap C. Ovarian Cancer—Insights into Platinum Resistance and Overcoming It. Medicina. 2023;10;59(3):544. doi.org/ 10.3390/medicina59030544.
2. Fletcher R, Powell MJ. A rapidly convergent descent method for minimization. The computer journal. 1963;6(2):163-8. doi.org/10.1093/comjnl/6.2.163.
3. Elmore S. Apoptosis: a review of programmed cell death. Toxicologic pathology. 2007;35(4):495-516. doi.org/10.1080/01926230701320337.
4. Shamas-Din A, Kale J, Leber B, Andrews DW. Mechanisms of action of Bcl-2 family proteins. Cold Spring Harbor perspectives in biology. 2013;5(4):a008714. doi: 10.1101/cshperspect.

a008714.
5. Oxford SM, Dallman CL, Johnson PW, Ganesan A, Packham G. Current strategies to target the anti-apoptotic Bcl-2 protein in cancer cells. Current medicinal chemistry. 2004;11(8):1031-40. doi.org/10.2174/0929867043455486.
6. Yoshimine S, Kikuchi E, Kosaka T, Mikami S, Miyajima A, Okada Y, Oya M. Prognostic significance of Bcl-xL expression and efficacy of Bcl-xL targeting therapy in urothelial carcinoma. British journal of cancer. 2013;108(11):2312-20. doi.org/ 10.1038/bjc.2013.216.
7. Scherr AL, Mock A, Gdynia G, Schmitt N, Heilig CE, Korell F, Rhadakrishnan P, Hoffmeister P, Metzeler KH, Schulze-Osthoff K, Illert AL. Identification of BCL-XL as highly active survival factor and promising therapeutic target in colorectal cancer. Cell death & disease. 2020;11(10):875. doi.org/10.1038/s41419-020-03092-7.
8. Zhang J, Bowden GT. Targeting Bcl-XL for prevention and therapy of skin cancer. Molecular Carcinogenesis: Published in cooperation with the University of Texas MD Anderson Cancer Center. 2007;46(8):665-70. doi.org/10.1002/mc.20330.
9. Jacobo-Herrera N, Pйrez-Plasencia C, Castro-Torres VA, Martнnez-V6zquez M, Gonz6lez-Esquinca AR, Zentella-Dehesa A. Selective acetogenins and their potential as anticancer agents. Frontiers in Pharmacology. 2019;10:447551. doi.org/10.3389/fphar.2019.00783.
10. Champy P, Huglinger GU, Fйger J, Gleye C, Hocquemiller R, Laurens A, Guйrineau V, Laprйvote O, Medja F, Lombиs A, Michel PP. Annonacin, a lipophilic inhibitor of mitochondrial complex I, induces nigral and striatal neurodegeneration in rats: possible relevance for atypical parkinsonism in Guadeloupe. Journal of neurochemistry. 2004;88(1):63-9. doi.org/10.1046/j.1471-4159.2003.02138.x.
11. Fujimoto Y, Murasaki C, Kakinuma K, Eguchi T, Ikekawa N, Furuya M, Hirayama K, Ikekawa T, Sahai M, Gupta YK, Ray AB. Squamostatin-A: unprecedented bis-tetrahydrofuran acetogenin from Annona squamosa. Tetrahedron letters. 1990;31(4):535-8. doi.org/10.1016/0040-4039(90)87027-W.
12. Liaw CC, Chang FR, Lin CY, Chou CJ, Chiu HF, Wu MJ, Wu YC. New Cytotoxic Monotetrahydrofuran Annonaceous Acetogenins from Annona muricata. Journal of natural products. 2002;65(4):470-5. doi.org/10.1021/np0105578.
13. Grinevicius VM, Andrade KS, Mota NS, Bretanha LC, Felipe KB, Ferreira SR, Pedrosa RC. CDK2 and Bcl-xL inhibitory mechanisms by docking simulations and anti-tumor activity from piperine enriched supercritical extract. Food and chemical toxicology. 2019;132:110644. doi.org/10.1016/j.fct.2019.110644.
14. Lessene G, Czabotar PE, Sleebs BE, Zobel K, Lowes KN, Adams JM, Baell JB, Colman PM, Deshayes K, Fairbrother WJ, Flygare JA. Structure-guided design of a selective BCL-XL inhibitor. Nature chemical biology. 2013;9(6):390-7. doi.org/10.1038/nchembio.1246.
15. BIOVIA, Dassault Systиmes, [Discovery studio visualizer], [v21.1.0.20298], San Diego: Dassault Systиmes; 2020. Available from https://www.3ds.com/products/biovia/discovery-studio/visualization.
16. Waterhouse A, Bertoni M, Bienert S, Studer G, Tauriello G, Gumienny R, Heer FT, de Beer TA, Rempfer C, Bordoli L, Lepore R. SWISS-MODEL: homology modelling of protein structures and complexes. Nucleic acids research. 2018;46(W1):W296-303. doi.org/10.1093/nar/gky427.
17. Laskowski RA, MacArthur MW, Thornton JM. PROCHECK: validation of protein structure coordinates, in International Tables of Crystallography, Volume F. Crystallography of Biological Macromolecules, eds. Rossmann M G & Arnold E, Dordrecht, Kluwer Academic Publishers, The Netherlands, 2001; 722-725. Available from https://onlinelibrary.wiley.com/iucr/itc/Fa/ch25o2v0001/sec25o2o6/
18. Nordin N, Khimani K, Abd Ghani MF. Acetogenins exhibit potential BCL-XL Inhibitor for the Induction of apoptosis in the molecular docking study. Current drug discovery technologies. 2021;18(6):98-108. doi.org/10.2174/1570163818666210204202426.
19. Morris GM, Huey R, Lindstrom W, Sanner MF, Belew RK, Goodsell DS, Olson AJ. Autodock4 and AutoDockTools4: automated docking with selective receptor flexibility. Journal of computational chemistry. 2009;30: 2785-2791. doi.org/10.1002/jcc.21256.
20. Hevener KE, Zhao W, Ball DM, Babaoglu K, Qi J, White SW, Lee RE. Validation of molecular docking programs for virtual screening against dihydropteroate synthase. Journal of chemical information and modeling. 2009;49(2):444-60. doi.org/10.1021/ci800293n.
21. Ferrari IV. Open access in silico tools to predict the ADMET profiling and PASS (Prediction of Activity Spectra for Substances of Bioactive compounds of Garlic (Allium sativum L.). BioRxiv. 2021:2021-07. doi.org/10.1101/2021.07.18.452815.
22. Eberhardt J, Santos-Martins D, Tillack AF, Forli S. AutoDock Vina 1.2. 0: New docking methods, expanded force field, and python bindings. Journal of chemical information and modeling. 2021;61(8):3891-8. doi.org/10.1021/acs.jcim.1c00203.
23. Lipinski CA, Lombardo F, Dominy BW, Feeney PJ. Experimental and computational approaches to estimate solubility and permeability in drug discovery and development settings. Advanced drug delivery reviews. 1997;23(1-3):3-25. doi.org/

10.1016/j.addr.2012.09.019.
24. Shargel L, Wu-Pong S. Andrew Yu. Applied biopharmaceutics and pharmacokinetics. 2015. Available from https://accesspharmacy.mhmedical.com/book.aspx?bookID=1592.
25. Ertl P, Schuffenhauer A. Estimation of synthetic accessibility score of drug-like molecules based on molecular complexity and fragment contributions. Journal of cheminformatics. 2009;1:1-1. doi:10.1186/1758-2946-1-8.
26. Patlewicz G, Jeliazkova N, Safford RJ, Worth AP, Aleksiev B. An evaluation of the implementation of the Cramer classification scheme in the Toxtree software. SAR and QSAR in Environmental Research. 2008;19(5-6):495-524. doi.org/10.1080/10629360802083871.
27. Lee TS, Cerutti DS, Mermelstein D, Lin C, LeGrand S, Giese TJ, Roitberg A, Case DA, Walker RC, York DM. GPU-accelerated molecular dynamics and free energy methods in Amber18: performance enhancements and new features. Journal of chemical information and modeling. 2018;58(10):2043-50. doi.org/10.1021/acs.jcim.8b00462.
28. Lindorff-Larsen K, Piana S, Palmo K, Maragakis P, Klepeis JL, Dror RO, Shaw DE. Improved side-chain torsion potentials for the Amber ff99SB protein force field. Proteins: Structure, Function, and Bioinformatics. 2010;78(8):1950-8. doi.org/10.1002/prot.22711.
29. Wang J, Wolf RM, Caldwell JW, Kollman PA, Case DA. Development and testing of a general amber force field. Journal of computational chemistry. 2004;25(9):1157-74. doi.org/10.1002/jcc.20035.
30. Darden T, York D, Pedersen L. Particle mesh Ewald: An N log (N) method for Ewald sums in large systems. The Journal of chemical physics. 1993;98(12):10089-92. doi.org/10.1063/1.464397.
31. Krдutler V, Van Gunsteren WF, Hьnenberger PH. A fast SHAKE algorithm to solve distance constraint equations for small molecules in molecular dynamics simulations. Journal of computational chemistry. 2001;22(5):501-8. doi.org/10.1002/1096-987X(20010415)22:5<501::AID-JCC1021>3.0.CO;2-V
32. Humphrey W, Dalke A, Schulten K. VMD: visual molecular dynamics. Journal of molecular graphics. 1996;14(1):33-8. doi.org/10.1016/0263-7855(96)00018-5.
33. Roe DR, Cheatham III TE. PTRAJ and CPPTRAJ: software for processing and analysis of molecular dynamics trajectory data. Journal of chemical theory and computation. 2013;9(7):3084-95. doi.org/10.1021/ct400341p.
34. Filimonov DA, Lagunin AA, Gloriozova TA, Rudik AV, Druzhilovskii DS, Pogodin PV, Poroikov VV. Prediction of the biological activity spectra of organic compounds using the PASS online web resource. Chemistry of Heterocyclic Compounds. 2014;50:444-57. doi.org/10.1007/s10593-014-1496-1.
35. Zhou Y, Zou J, Xu J, Zhou Y, Cen X, Zhao Y. Recent advances of mitochondrial complex I inhibitors for cancer therapy: Current status and future perspectives. European Journal of Medicinal Chemistry. 2023;251:115219. doi.org/10.1016/j.ejmech.2023.115219.
36. Nandi S, Khatua S, Nag A, Sen S, Chakraborty N, Naskar A, Acharya K, Mekky RH, del Mar Contreras M, Calina D, Dini I. Dolastatins and their analogues present a compelling landscape of potential natural and synthetic anticancer drug candidates. Current Research in Biotechnology. 2023;14:100167. doi.org/10.1016/j.crbiot.2023.100167.
37. Srivastava N, Saxena AK. Caspase-3 activators as anticancer agents. Current Protein and Peptide Science. 2023;24(10):783-804. doi.org/10.2174/1389203724666230227115305.
38. Derbrй S, Duval R, Rouй G, Garofano A, Poupon E, Brandt U, Susin SA, Hocquemiller R. Semisynthesis and Screening of a Small Library of Pro-Apoptotic Squamocin Analogues: Selection and Study of a Benzoquinone Hybrid with an Improved Biological Profile. ChemMedChem: Chemistry Enabling Drug Discovery. 2006;1(1):118-29. doi.org/10.1002/cmdc.200500011.
39. Anderson RL, Balasas T, Callaghan J, Coombes RC, Evans J, Hall JA, Kinrade S, Jones D, Jones PS, Jones R, Marshall JF. A framework for the development of effective anti-metastatic agents. Nature Reviews Clinical Oncology. 2019;16(3):185-204. doi.org/10.1038/s41571-018-0134-8.
40. Ferreira LG, Dos Santos RN, Oliva G, Andricopulo AD. Molecular docking and structure-based drug design strategies. Molecules. 2015;20(7):13384-421. doi.org/10.3390/molecules200713384.
41. Abd Ghani MF, Othman R, Nordin N. Molecular docking study of naturally derived flavonoids with antiapoptotic BCL-2 and BCL-XL proteins toward ovarian cancer treatment. Journal of Pharmacy and Bioallied Sciences. 2020;12(Suppl 2):S676-80. doi: 10.4103/jpbs.JPBS_272_19
42. Baell J, Walters MA. Chemistry: Chemical con artists foil drug discovery. Nature. 2014;513(7519):481-3. doi.org/10.1038/513481a.
43. Zanger UM, Schwab M. Cytochrome P450 enzymes in drug metabolism: regulation of gene expression, enzyme activities, and impact of genetic variation. Pharmacology & therapeutics. 2013;138(1):103-41. doi.org/10.1016/j.pharmthera.2012.12.007.
44. Koirala M, DiPaola M. Overcoming Cancer Resistance: Strategies and Modalities for Effective Treatment. Biomedicines. 2024;12(8):1801. doi.org/ 10.3390/biomedicines12081801.
45. Ertl P, Schuffenhauer A. Estimation of synthetic accessibility score of drug-like molecules based on molecular complexity and fragment contributions.

Journal of cheminformatics. 2009;1:1-1. doi.org/10.1186/1758-2946-1-8.
46. King-Smith E, Zwick III CR, Renata H. Applications of oxygenases in the chemoenzymatic total synthesis of complex natural products. Biochemistry. 2018;57(4):403-12. doi.org/10.1021/acs.biochem.7b00998.
47. Zou H, Yang Y, Chen HW. Natural compounds ursolic acid and digoxin exhibit inhibitory activities to cancer cells in RORγ-dependent and-independent manner. Frontiers in Pharmacology. 2023;14:1146741. doi.org/10.3389/fphar.2023.1146741.
48. Patel P, Panda PK, Kumari P, Singh PK, Nandi A, Mallick MA, Das B, Suar M, Verma SK. Selective in vivo molecular and cellular biocompatibility of black peppercorns by piperine-protein intrinsic atomic interaction with elicited oxidative stress and apoptosis in zebrafish eleuthero embryos. Ecotoxicology and Environmental Safety. 2020;192:110321. doi.org/10.1016/j.ecoenv.2020.110321.
49. Seeliger D, de Groot BL. Conformational transitions upon ligand binding: Holo structure prediction from apo conformations. Biophysical Journal. 2010;98(3):428a. doi: 10.1016/j.bpj.2009.12.2318
50. Johnson DK, Karanicolas J. Selectivity by small-molecule inhibitors of protein interactions can be driven by protein surface fluctuations. PLoS computational biology. 2015 Feb 23;11(2):e1004081. doi.org/10.1371/journal.pcbi.1004081.